An Improved Volume-of-Fluid Method for Wave Impact

Kleefsman, K.M. Theresa; Veldman, Arthur E.P.

Published in:
EPRINTS-BOOK-TITLE

Link to publication in University of Groningen/UMCG research database

AN IMPROVED VOLUME-OF-FLUID METHOD FOR WAVE IMPACT

K.M.Theresa Kleefsman★, Arthur E.P. Veldman★

★Department of Mathematics and Computing Science, University of Groningen
P.O. Box 800 , 9700 AV Groningen, The Netherlands
e-mails: theresa@math.rug.nl, veldman@math.rug.nl

Key words: Wave loading; moving body; numerical simulation; Cartesian grid; volume-of-fluid; computational fluid dynamics.

Abstract. *This paper describes a modified volume-of-fluid method for the simulation of wave impact problems at moving bodies. The method is based on the Navier-Stokes equations that describe the motion of incompressible viscous fluid flow. The equations are discretised on a fixed Cartesian grid using a finite volume method. The geometry of the body is piecewise linear, resulting in cut cells. The displacement of the free surface is done using the volume-of-fluid method combined with a local height function to prevent flotsam and jetsam. In this paper some validation results of the method are presented. First, the method has been tested on the simulation of steep waves. Second, a breaking dam flow has been simulated, where the results are compared with available experimental measurements. Finally, results of a simulation of green water on the deck of a moving ship are shown.*

1

1 INTRODUCTION

There is a great need for calculation methods for local phenomena of wave impact loading and loading from green water on the deck of a ship. Most of the existing methods are not capable of predicting the local loads. Part of the Joint Industry Project SafeFLOW, initiated in January 2001, is devoted to the development of a CFD method which is able to predict local wave impact on floaters operating in the offshore industry.

The development of the method, called COMFLOW, has started in 1995 with the simulation of liquid-filled spacecraft that are tumbling in space [5, 4]. In this application where the surface tension is the driving force, a good handling of the free surface is crucial. The method has also been applied to blood flow through (elastic) arteries, where the moving elastic vessel wall is in a numerical sense similar to a free liquid surface [8]. A rather new application was found in the maritime world where sloshing inside anti-roll tanks has been simulated. In 1999 a pilot study of the simulation of green water on the deck of a fixed vessel with dambreak starting situation of the fluid has been performed, to investigate if the method is capable of capturing the local flow details on the deck [2]. Because of promising results, it was decided to move on in this direction in the SafeFLOW project.

The simulation of fluid flow in COMFLOW is based on the Navier-Stokes equations for an incompressible, viscous fluid. The equations are discretised using the finite volume method. For the displacement of the free surface the VOF method has been used adapted with a local height function. A good choice of the discrete boundary conditions at the free surface is found to be very important for robustness and accuracy of the method.

In this paper, the model used in COMFLOW is described. To test the capabilities of the method in the simulation of steep waves, results of a steep wave event without an object in the flow are presented. Also results are shown of simulations for a dambreak with a box in the flow. This simulation can be seen as a model of the water flow on the deck of a ship due to green water. Finally, results are shown of a simulation of green water on the deck of a moving vessel compared with measurements.

2 GOVERNING EQUATIONS

Flow of a homogeneous, incompressible, viscous fluid is described by the continuity equation and the Navier-Stokes equations. The continuity equation describes conservation of mass and the Navier-Stokes equations describe conservation of momentum. In conservative form, they are given by

$$\oint_{\partial V} \boldsymbol{u} \cdot \boldsymbol{n} dS \;=\; 0, \tag{1}$$

$$\int_V \frac{\partial \boldsymbol{u}}{\partial t} dV + \oint_{\partial V} \boldsymbol{u}\boldsymbol{u}^{\mathrm{T}} \cdot \boldsymbol{n} dS \;=\; -\frac{1}{\rho} \oint_{\partial V} (p\boldsymbol{n} - \mu \nabla \boldsymbol{u} \cdot \boldsymbol{n}) dS + \int_V \boldsymbol{F} dV. \tag{2}$$

Here, ∂V is the boundary of volume V, $\boldsymbol{u} = (u, v, w)$ is the velocity vector in the three coordinate directions, $\boldsymbol{n}$ is the normal at the boundary ∂V, ρ denotes the density, p is the pressure, ∇ is the gradient operator. Further μ denotes the dynamic viscosity and $\boldsymbol{F} = (F_x, F_y, F_z)$ is an external body force, for example gravity.

In the case that moving rigid bodies are present in the domain V, the above equations still hold, with the additional condition that the fluid velocity at the boundary of the object is equal to the object velocity.

2.1 Boundary conditions

At the solid walls of the computational domain and at the objects inside the domain, a no-slip boundary condition is used. This condition is described by $\boldsymbol{u} = 0$ for fixed boundaries, and $\boldsymbol{u} = \boldsymbol{u}_b$ for moving objects with $\boldsymbol{u}_b$ the object velocity.

Some of the domain boundaries may let fluid flow in or out of the domain. Especially, when performing wave simulations, an inflow boundary is needed where the incoming wave is prescribed and at the opposite boundary a non-reflecting outflow condition should be used. In our method, the wave on the inflow boundary can be prescribed as a regular linear wave or a regular 5th order Stokes wave. Also a superposition of linear components can be used which results in an irregular wave. At the outflow boundary, a Sommerfeld condition is very appropriate in cases where a regular wave is used. In the case of an irregular wave or a much deformed regular wave (e.g. due to the presence of an object in the flow) a damping zone is added at the end of the domain [11].

2.2 Free surface

If the position of the free surface is given by $s(x, t) = 0$, the displacement of the free surface is described using the following equation

$$\frac{Ds}{Dt} = \frac{\partial s}{\partial t} + (u \cdot \nabla)s = 0. \tag{3}$$

At the free surface, boundary conditions are necessary for the pressure and the velocities. Continuity of normal and tangential stresses leads to the equations

$$-p + 2\mu \frac{\partial u_n}{\partial n} = -p_0 + 2\gamma H \tag{4}$$

$$\mu \left(\frac{\partial u_n}{\partial t} + \frac{\partial u_t}{\partial n} \right) = 0. \tag{5}$$

Here, u_n is the normal component of the velocity, p_0 is the atmospheric pressure, γ is the surface tension and $2H$ denotes the total curvature.

3 NUMERICAL MODEL

To solve the Navier-Stokes equations numerically, the computational domain is covered with a fixed Cartesian grid. The variables are staggered, which means that the velocities

3

are defined at cell faces, whereas the pressure is defined in cell centers.

The body geometry is piecewise linear and cuts through the fixed rectangular grid. Volume apertures (F^b) and edge apertures (A^x, A^y, and A^z) are used to indicate for each cell which part of the cell and cell face respectively is open for fluid and which part is blocked by solid geometry. To track the free surface, the volume-of-fluid function F^s is used, which is 0 if no fluid is present in the cell, 1 if the cell is completely filled with fluid and between 0 and 1 if the cell is partly filled with fluid.

The Navier-Stokes equations are solved in every cell containing fluid. Cell labeling is introduced to distinguish between cells of different characters. First the cells which are completely blocked by geometry are called B(oundary) cells. These cells have volume aperture F^b=0. Then the cells which are empty, but have the possibility of letting fluid flow in are labeled E(mpty). The adjacent cells, containing fluid, are S(urface) cells. The remaining cells are labeled as F(luid) cells. Note that these cells do not have to be completely filled with fluid. In Figure 1 an example of the labeling is given.

Figure 1: Cell labeling: dark grey denotes solid body, light grey is liquid

3.1 Discretisation of the continuity equation

The continuity and Navier-Stokes equations are discretised using the finite volume method. The natural form of the equations when using the finite volume method is the conservative formulation as given in Eq. (1) and (2). In this paper, the discretisation is explained in two dimensions. In most situations, this can be extended to three dimensions in a straightforward manner. In Figure 2 a computational cell is shown, which is cut by the geometry of a moving body. When applying conservation of mass in this cell, the discretisation results in

$$
\begin{aligned}
u_e A_e^x \delta y \;+\; v_n A_n^y \delta x \;-\; u_w A_x^w \delta y \;-\; v_s A_s^y \delta x \;+\; \\
u_b (A_e^x - A_w^x)\delta y \;+\; v_b (A_n^y - A_s^y)\delta x \;=\; 0,
\end{aligned}
\tag{6}
$$

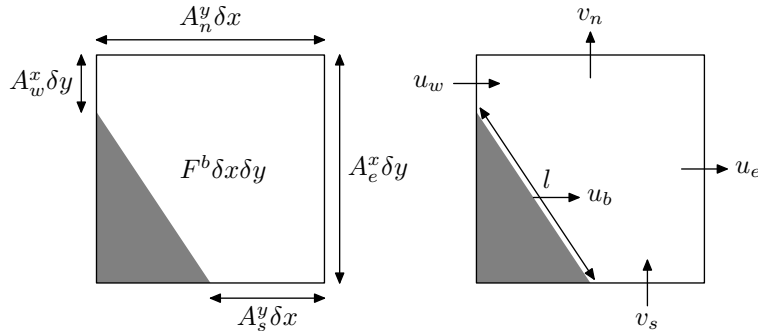where the notation is explained in Figure 2.

Figure 2: Conservation cell for the continuity equation

3.2 Discretisation of the Navier-Stokes equations

For the discretisation of the Navier-Stokes equations, control volumes are defined containing velocities which are defined on cell faces. In the case of uncut cells, the control volume of a velocity simply consists of the right half of the cell left of the velocity and the left half of the cell right of the velocity. In case of cut cells the procedure to define control volumes has been explained in detail in [4].

The time derivative in the Navier-Stokes equations is discretised in space using the midpoint rule. This results in

$$
\int_V \frac{\partial u}{\partial t} dV \doteq \frac{\partial u_c}{\partial t} F_c^b \delta x_c \delta y \tag{7}
$$

Here, u_c is the central velocity around which the control volume is placed and $F_c^b \delta x_c \delta y$ is the volume of the control volume.

The convective term is discretised directly from the boundary integral which is given by

$$
\oint_{\partial V} u \boldsymbol{u} \cdot \boldsymbol{n} dS. \tag{8}
$$

Note, that this integral contains two different velocities: the scalar velocity u is advected with the velocity vector $\boldsymbol{u}$. This integral is evaluated along all boundaries of the control volume by multiplying the scalar velocity u with the mass flux through the boundary $\boldsymbol{u} \cdot \boldsymbol{n} dS$. Consequently, the discretisation of the convective term results in a matrix that is skew symmetric, which is also a property of the continuous convective operator [10].

The diffusive term, which for the Navier-Stokes equation in x-direction is given by

$$
\frac{1}{\rho} \oint_{\partial V} \mu \frac{\partial u}{\partial \boldsymbol{n}} dS, \tag{9}
$$

is discretised along all boundaries of the control volume. To ensure stability, the term $\frac{\partial u}{\partial \boldsymbol{n}}$ is discretised in cut-cells as if the cells are uncut. The error introduced this way is small

5

and has no influence in the convection-dominated simulations. The discretisation results in a symmetric matrix that is negative definite.

The pressure term is discretised as a boundary integral, resulting for the Navier-Stokes equation in x-direction in

$$\oint_{\partial V} p n_x dS \doteq (p_e - p_w) A_c^x \delta y. \tag{10}$$

Here, p_e and p_w are the pressure in the eastern and western cell respectively, A_c^x is the edge aperture of the cell face where the central velocity is defined. In this way, the discrete gradient operator becomes the transpose of the discrete divergence operator in the continuity equation.

The external force is discretised similar to the time derivative, resulting for the x-direction in

$$\int_V F_x dV \doteq F_{x_c} F_c^b \delta x_c \delta y. \tag{11}$$

Here, F_{x_c} is the force at the location of the central velocity.

Detailed explanations of the discretisations described in this section are given in [4] and [3].

3.3 Temporal discretisation

The continuity and Navier-Stokes equations are discretised in time using the forward Euler method. This first order method is accurate enough, because the order of the overall accuracy is already determined by the first order accuracy of the free surface displacement algorithm. Using superscript n for the time level, the temporal discretisation results in

$$M \boldsymbol{u}_h^{n+1} = 0, \tag{12}$$

$$\Omega \frac{\boldsymbol{u}_h^{n+1} - \boldsymbol{u}_h^n}{\delta t} + C(\boldsymbol{u}_h^n) \boldsymbol{u}_h^n = -\frac{1}{\rho}(M^{\mathrm{T}} \boldsymbol{p}_h^{n+1} - \mu D \boldsymbol{u}_h^n) + \boldsymbol{F}_h^n. \tag{13}$$

The continuity equation is discretised at the new time level to ensure a divergence free velocity field. The spatial discretisation is written in matrix notation where M is the divergence operator, Ω contains cell volumes, C contains the convection coefficients (which depend on the velocity vector) and D contains diffusive coefficients.

3.4 Solution method

To solve the system of equations, the equations are rearranged to

$$\boldsymbol{u}_h^{n+1} = \tilde{\boldsymbol{u}}_h^n + \delta t \Omega^{-1} \frac{1}{\rho} M^{\mathrm{T}} \boldsymbol{p}_h^{n+1}, \tag{14}$$

where

$$\tilde{\boldsymbol{u}}_h^n = \boldsymbol{u}_h^n - \delta t \Omega^{-1}(C(\boldsymbol{u}_h^n) \boldsymbol{u}_h^n - \frac{\mu}{\rho} D \boldsymbol{u}_h^n - \boldsymbol{F}_h^n). \tag{15}$$

6

First, an auxiliary vector field $\tilde{\boldsymbol{u}}_h^n$ is calculated using Eq. (15). Next, Eq. (14) is substituted in Eq. (12) which results in a Poisson equation for the pressure. From this equation the pressure is solved using the SOR (Successive Over Relaxation) method where the optimal relaxation parameter is determined during the iterations [1]. Once the pressure field is known, the new velocity field is calculated from $\tilde{\boldsymbol{u}}_h^n$ using the pressure gradient.

3.5 Free surface displacement

After the new velocity field has been calculated, the free surface can be displaced. This is done using an adapted version of the volume-of-fluid method first introduced by [7]. A piecewise constant reconstruction of the free surface is used, where the free surface is displaced by changing the VOF value in a cell using calculated fluxes through cell faces.

The original VOF method has two main drawbacks. The first is that flotsam and jetsam can appear, which are small droplets disconnecting from the free surface [9]. The other drawback is the gain or loss of water due to rounding of the VOF function. By combining the VOF method with a local height function [4], these problems do not appear any more. The local height function is adopted in the following way. For every surface cell, locally a height function is defined, which gives the height of the water in a column of three cells as in Figure 3. The direction in which the function is defined is the direction of the coordinate axis that is most normal to the free surface. Then not the individual fluxes of the three cells are updated, but the height function is updated using fluxes through the boundaries of the column of the three cells (the dashed-lined region in Figure 3). The individual VOF values of the three cells are then calculated from the height of the water in the column. When using this adopted fluid-displacement algorithm, the method is strictly mass conservative and almost no flotsam and jetsam appear.
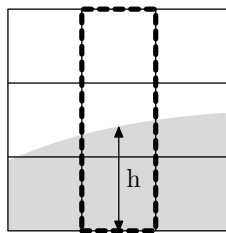

Figure 3: The VOF function in cells near surface cells is updated using a local height function

3.6 Free surface boundary conditions

At the free surface, boundary conditions are needed for the pressure and the velocities. The pressure in surface cells is calculated as an interpolation or extrapolation from the pressure in an adjacent fluid cell and the boundary condition at the free surface.

The velocities in the neighbourhood of the free surface can be grouped in different

classes (see Figure 4). The first class contains the velocities between two F-cells, between

E	E	E	S
S	S	S	F
S	F	F	F

FF, FS, SS: momentum equation

SE: extrapolation

EE: tangential free surface condition

Figure 4: Different characters of velocities near the free surface

two S-cell and between an S and F cell. These velocities are determined by solving the momentum equation, so the velocities are called momentum velocities. The second class consists of velocities between two E cells which are sometimes needed to solve the momentum equation. These are determined using the tangential free surface condition. The last class consists of velocities between surface and empty cells (SE-velocities).

The choice for SE-velocities has a large influence on the accuracy and robustness of the method. In the original MAC-method, the SE-velocities are determined by demanding conservation of mass in surface cells [6]. A large disadvantage of this method is, that when cells are cut by the geometry, the resulting SE-velocity calculated from conservation of mass in the S-cell can get very large due to a small edge aperture (see the left of Figure 5). This causes major stability problems when such a configuration stays the same for several adjacent time steps. Therefore, this method has not been adopted in our cut-cell method. Instead, an extrapolation method is proposed, where the SE-velocities are extrapolated from the direction of the main body of the fluid. For accurate wave simulations, a linear extrapolation would be best (see the right of Figure 5), but this causes problems when the velocity field is not smooth. Therefore, a combination of linear and constant extrapolation is used, depending on the smoothness of the local velocity field.

3.7 Stability of the numerical method

In the case of uncut cells with fixed objects, the stability of the equation containing the time integration term and the convective term is given by the CFL-restriction $\frac{\delta t|u|}{h} \leq$ 1. Here, h is the size of the uncut cell. When cut cells are present, this criterion is not changed. This result is not directly straightforward when looking at the equation containing the time derivative and the convective term

$$\frac{\partial \boldsymbol{u}}{\partial t} = -\Omega^{-1}C(\boldsymbol{u}, \boldsymbol{u}_b)\boldsymbol{u} \tag{16}$$

where $\boldsymbol{u}_b$ is the object velocity. The matrix Ω is a diagonal matrix containing the volumes of the cells, so these entries can become arbitrary small for cut cells. So the elements in the matrix Ω^{-1} can become arbitrary large. But, when estimating the eigenvalues of the
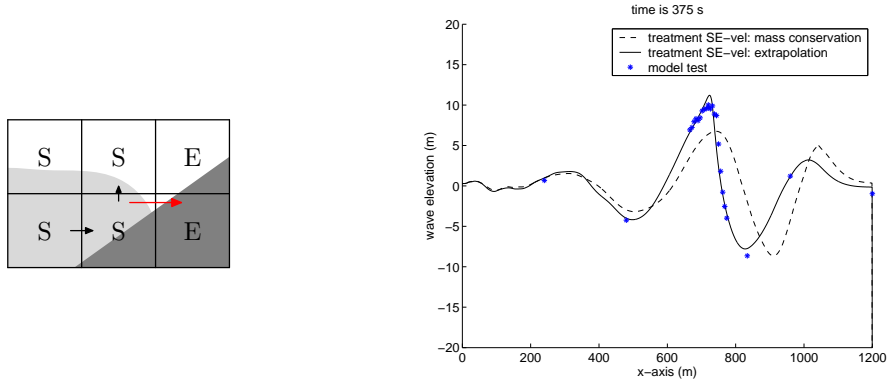
Figure 5: Left: very large SE-velocity when using mass conservation; right: different methods for SE-velocities in a steep wave simulation

convective matrix C using Gerschgorin circles by being order $O(\frac{\Omega}{h}u)$ (so the eigenvalues of $\Omega^{-1}C$ are of order $O(\frac{u}{h})$), it can be concluded that the same stability criterion is needed as for the uncut-cells case [3].

When moving objects are present, the story becomes somewhat different. Now, the CFL-criterion does not guarantee stability anymore, because the eigenvalues of $\Omega^{-1}C(\boldsymbol{u}, \boldsymbol{u}_b)$ are of order $O(\Omega^{-1}h\boldsymbol{u}_b)$ which means that they can become arbitrary large due to the arbitrary large entries of Ω^{-1}. To cancel the effect of Ω a formulation based on a weighted average of the fluid velocity and the boundary velocity should be applied in the cells cut by the moving object. To avoid smearing of the interface in cases where it is not necessary to stabilise the convective term, the following discretisation is used

$$\boldsymbol{u}^{n+1} = \Omega^{n+1}(\Omega^{n+1} + |\Delta\Omega|)^{-1}(\boldsymbol{u}^n + \delta t(\Omega^{n+1})^{-1}$$
$$(-C^n\boldsymbol{u}^n)) + (I - \Omega^{n+1}(\Omega^{n+1} + |\Delta\Omega|)^{-1})\boldsymbol{u}_b^{n+1} \qquad (17)$$

where $\Delta\Omega = \Omega^{n+1} - \Omega^n$ is the difference between Ω's at two different time steps. The factor $\Omega^{n+1}(\Omega^{n+1} + |\Delta\Omega|)^{-1}$ is chosen because then the stabilising term is only used when the body is moving; note that it equals unity for fixed objects. The maximal stabilisation is required when the object is moving normal to its boundary, whereas no stabilisation is needed when the object is moving tangential to its boundary (see Figure 6). A detailed explanation of the stability of the convective terms is given in [3].

From the diffusive term, also a stability criterion follows with a restriction on the time step. In the case of uncut cells, this criterion is given by $\delta t \leq \frac{h^2}{2\nu}$, where ν denotes kinematic viscosity. Because the diffusive term is discretised as if all cells were uncut ('staircase' approach), the above criterion is also valid in our model.

4 SIMULATION OF STEEP WAVE EVENTS

For the simulation of wave impact at for example the bow of a vessel, an accurate simulation of steep waves is necessary. Therefore, an irregular wave event that has been used
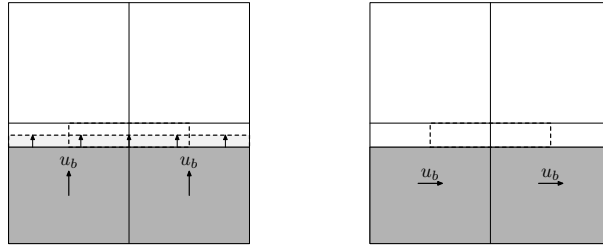
9

Figure 6: Left: boundary moving normal to itself: maximal stabilisation is required; right: boundary moving tangential to itself: no stabilisation is required

for bow impact experiments at the Maritime Research Institute Netherlands (MARIN) is chosen to be simulated with our numerical method. For comparison of the numerical results with the measurements, the wave should be prescribed at the inflow boundary such that the same wave results as in the experiment. Therefore, measurements of a wave probe 720 meter in front of the focusing point of the steep wave event have been used to start up the wave. The time series of the wave height at that wave probe have been analyzed using Fourier transformations. The linear components following from the analysis have been prescribed at the inflow boundary. Although the wave is not linear at that position, the wave prescription turned out to be accurate.

In this paper, results of the simulation of a wave event of a 1/16 steep wave in a sea state steepness for 100 year return period are shown. The wave is built in such a way, that on beforehand the position and time point where and when the wave is focusing are known. In the left of Figure 7, the time trace of the wave elevation at the focusing point is presented. The numerical prediction of wave height and steepness compare well with the experiment. This can also be seen from the right of Figure 7, where the spatial wave elevation has been shown at two different time points. At the time of 428 seconds, the predicted wave is a bit in front of the experiment.

Examining the results, it can be concluded that the current method is able to simulate a steep wave event.

5 DAMBREAK SIMULATION

At MARIN, experiments have been performed for breaking dam flows. These experiments can be seen as a simple model of green water flow on the deck of a ship. The dambreak is a very popular validation case, because the set up is easy, no special in- or outflow conditions are needed. A large tank of 3.22 by 1 by 1 meter is used with an open roof (scale 1:15). The right part of the tank is first closed by a door. Behind the door, 0.55 meter of water is waiting to flow into the tank when the door is opened. At a certain moment, a weight is released which opens the door. In the tank, a box is placed which is a scale model of a container on the deck of a ship.

During the experiment, measurements have been performed of water heights, pressures
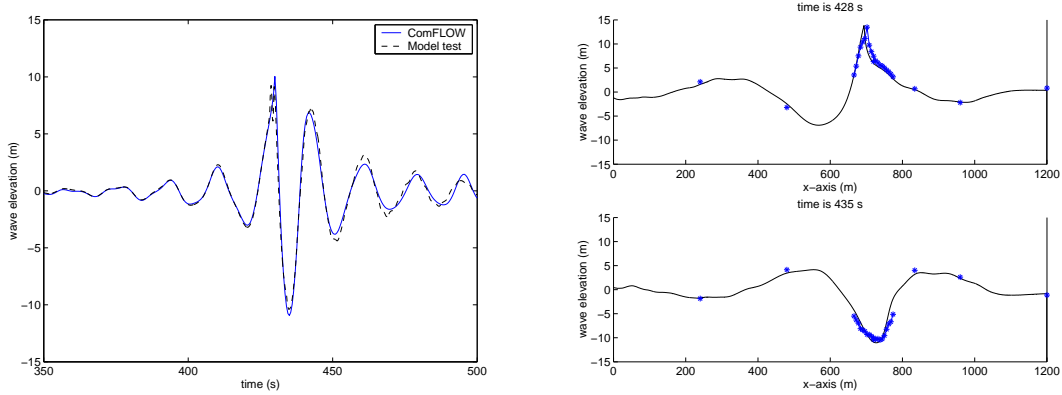
Figure 7: Steep wave event: wave elevation at 720 m behind the inflow boundary (left) and wave elevation at two different time points (right)
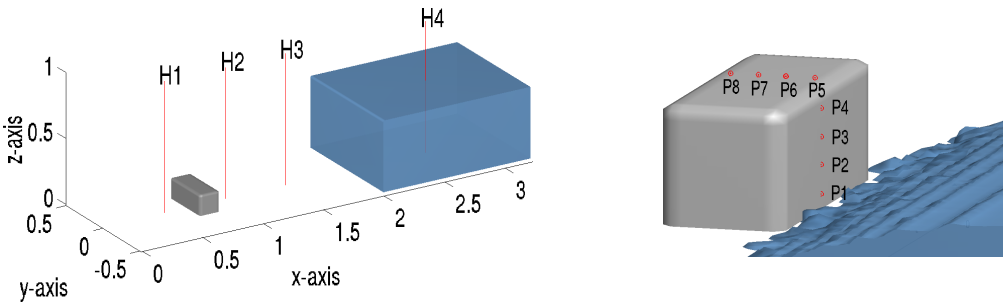

Figure 8: Measurement positions for water heights and pressures in the dambreak experiment

and forces. In Figure 8, the positions of the measured water heights and pressures are shown. Four vertical wave probes have been used: one in the reservoir and the other three in the tank. The box was covered by eight pressure pick-ups, four on the front of the box and four on the top. The forces on the box were also measured. To determine the velocity of the water when entering the tank, a horizonal wave probe is used near the side wall of the tank.

As initial configuration of the simulation with COMFLOW, the water in the right part of the domain is at rest. When the simulation is started, the water starts to flow into the empty tank due to gravity. In Figure 9 two snapshots of the early stages of the simulation are shown together with images of the video of the experiment (at the same moments in time). The smaller pictures inside the snapshots show the water in the reservoir. There is a very good agreement between simulation and experiment. The moment in time when the water is first hitting the box is the same. The shape of the free surface, bending a bit forwards in the second picture, is seen in both experiment and simulation. In the simulation, the free surface has some ripples that are due to the computational grid.

In Figure 10 the time history of the horizontal wave probe is shown, compared with the simulation. The first stage of the simulation compares very well with the experiment, the
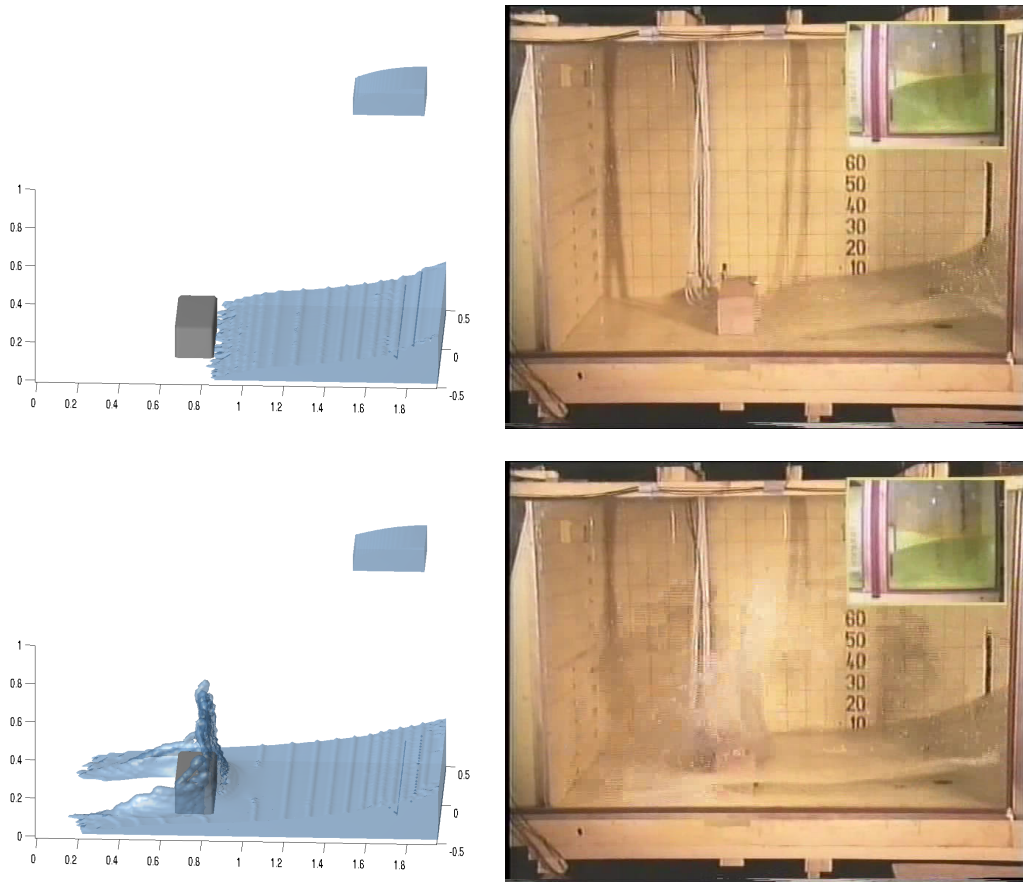
11

Figure 9: Snapshots of a dambreak simulation with a box in the flow compared with experiment at time 0.4 and 0.56 seconds

velocity with which the water is flowing into the tank is predicted very well. By the time the water hits the box, there is a difference between the experiment and the simulation. In the experiment, the water is slowed down: the wave probe is totally covered by water only after 2 seconds. In the simulation this is the case after 0.5 seconds. When looking at the movie of simulation and experiment, this difference is not present, suggesting an inconsistency in the wave probe measurements. The flow reaches the end wall at the same time in simulation and experiment. So the appearing difference in Figure 10 is not a real difference between simulation and experiment.

In Figure 11, the water height at two locations is shown: in the reservoir, and in the tank just in front of the box. The agreement in both pictures is very good until the water has returned from the back wall (after about 1.8 seconds). After that some differences occur, but the global behaviour is still the same. When the water has returned from the wall, the water height at probe H2 is largest. The water flows back to the reservoir, where it turns over again after about 4 seconds. The moment that this second wave meets the wave probe at H2 again is almost exactly the same in simulation and experiment.
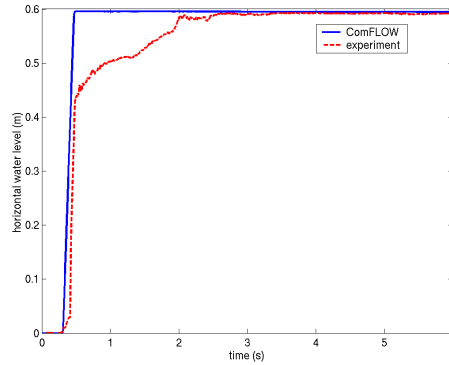
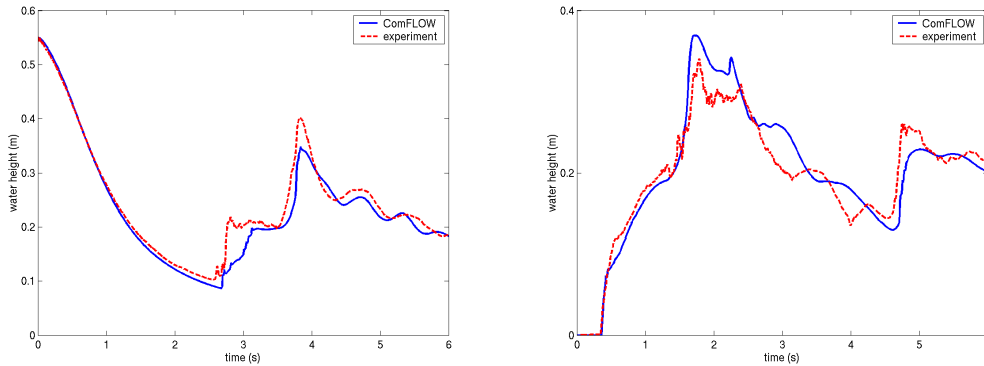Figure 10: Horizontal wave probe along the side of the tank

Figure 11: Vertical water heights in the reservoir H4 (left) and the tank H2 (right)

The moment the wave hits the box is perfectly captured by the simulation as can be seen from Figure 12. Here the pressure at point P1 and P3 at the front of the box and at the top of the box, P5 and P7 (see Figure 8), are shown. The magnitude of the impact pressure is the same for simulation and experiment at pressure point P1 (the lowest on the box), but is underpredicted by the simulation at point P3. The moment the return wave hits the box again (at about 4.7 seconds) is again visible in the graphs. In the bottom graphs of Figure 12, where the time history of pressure transducers at the top op the box are shown, a clear difference occurs between simulation and experiment. After about 1.3 seconds, there is a wiggle in the simulation with a duration of 0.5 seconds, which is not present in the experiment. Before this point, the water hits the top of the box when the wave coming back from the wall is overturning. This difference is a real difference that cannot be explained properly at the moment.

Several spikes appear in the pressure signals, which are spikes in all the graphs at the same moment. These spikes occur, because some water enters an empty cell that is
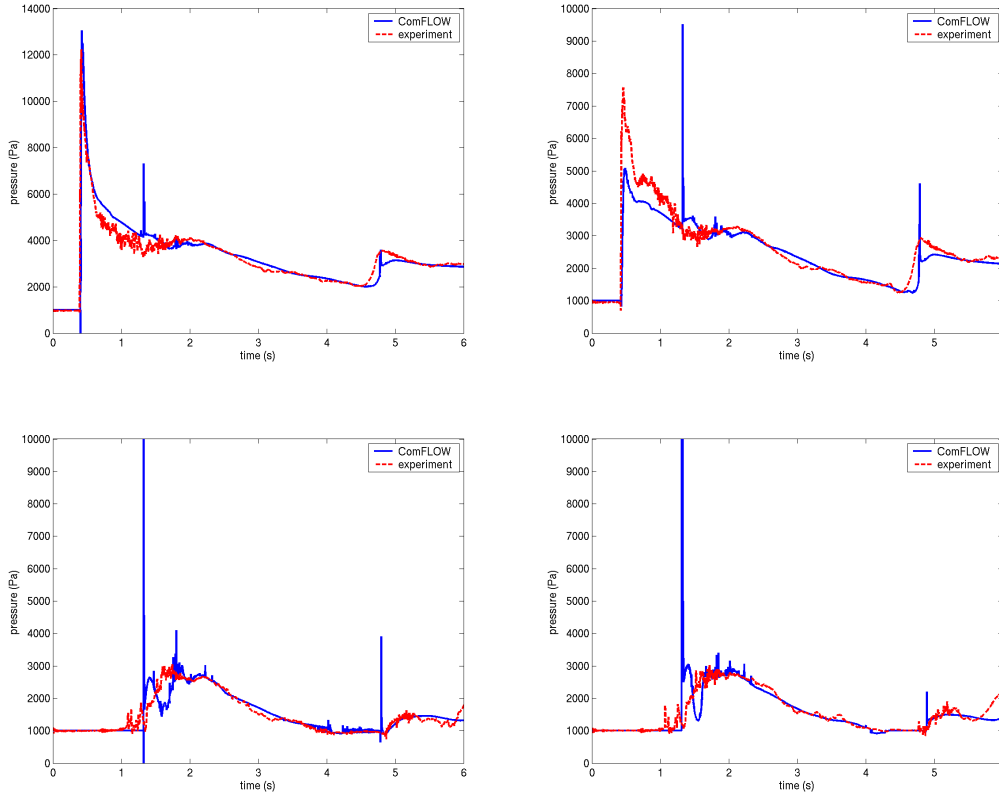
Figure 12: Pressure time histories of P1 (upper left), P3 (upper right), P5 (lower left), and P7 (lower right)

completely surrounded by cells with fluid. Then, this empty cell changes to a fluid cell in one time step without being a surface cell in between. This discontinuous change in label results in a pressure spike over the whole pressure field.

In Figure 13 a grid refinement study of the dambreak simulation is shown. Three different grids have been used with in increasing order 59x19x17 grid points, 118x38x34 grid points and 236x76x68 grid points. The finest grid has also been used in the previous figures. In the figure, the pressure along the lower part of the front side of the box is shown. The overall flow of the water is pretty much the same in all three grids, but when zooming in on the pressure peak (in the right of the figure), differences occur. The coarsest grid is clearly not good enough. The pressure peak is overpredicted and the water reaches the box too late. Although, the water reaches the box earlier in the finer grids, there is still a small difference between simulation and experiment. The magnitude of the impact is better predicted on the finer grids.

Concluding, the results of the dambreak simulation are in good agreement with the experiment. The global behaviour of the fluid is the same and the impact peak of the pressure agrees well, especially at the lower part of the box.
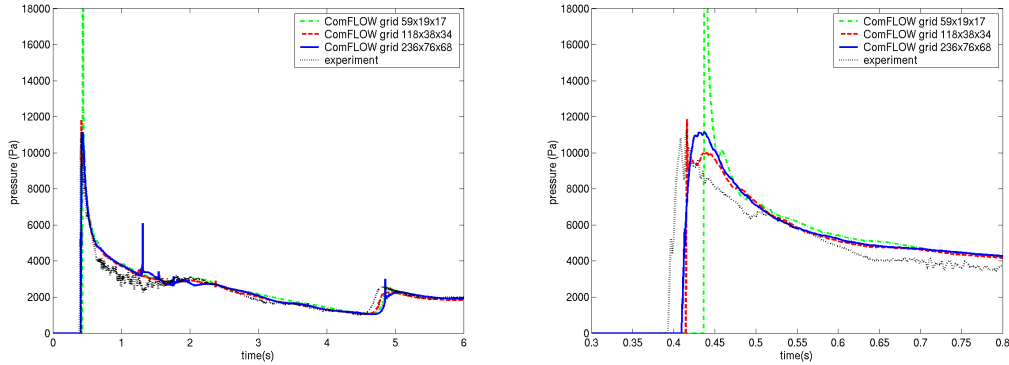
14

Figure 13: Grid refinement in the dambreak simulation: pressure at the lower part of the box, with on the right a zoomed picture

6   GREEN WATER ON THE DECK OF A MOVING FPSO

The ultimate test case for COMFLOW in the current project is the calculation of loads due to green water on the deck of a moving FPSO (Floating Production Storage and Offloading vessel). For validation, an experiment from the Greenwater JIP performed at MARIN has been used. Measurements were done of the wave in front of the FPSO, relative wave heights in the neighbourhood of the FPSO, water heights and pressures at the deck of the FPSO and the pressure at some places at a deck structure. The FPSO has a total length of 260 meter and is 47 meter wide. The draft is 16.5 meter, the total height of the deck at the fore side of the FPSO is 25.6 meter. There is a bulwark extension of 1.4 meter. At the deck, a box-like structure has been placed at which forces and pressures have been measured. The bow has a full elliptical shape without flare. The wave that has been chosen has a period of 12.9 seconds and the wave length is 260 meter, equal to the length of the FPSO. The wave amplitude is 6.76 meter. To be sure that the same wave has been used in the experiment and in the simulation, the wave measurement 230 meter in front of the bow of the vessel has been used to initiate the wave at the inflow boundary. The signal from the wave probe has been decomposed in linear components which are prescribed at the inflow boundary. The motion of the ship is prescribed using the measurements of the experiment. The simulation has been performed with only half of the FPSO in a relatively small domain around the bow of the vessel. A grid with 100x60x80 grid points has been used. In Figure 14 some snapshots of the simulation are shown during the first period of the simulation. The large wave is building in front of the vessel after which it starts to flow onto the deck. The water flows off the deck when the ship is straightening.

In Figure 15, the relative wave height in front of the vessel, is shown. In both pictures there is a good agreement, such that it can be concluded that the motion of the vessel relative to the wave motion does not differ much in simulation and experiment. The water height on the deck of the vessel has been compared in Figure 16. When the water
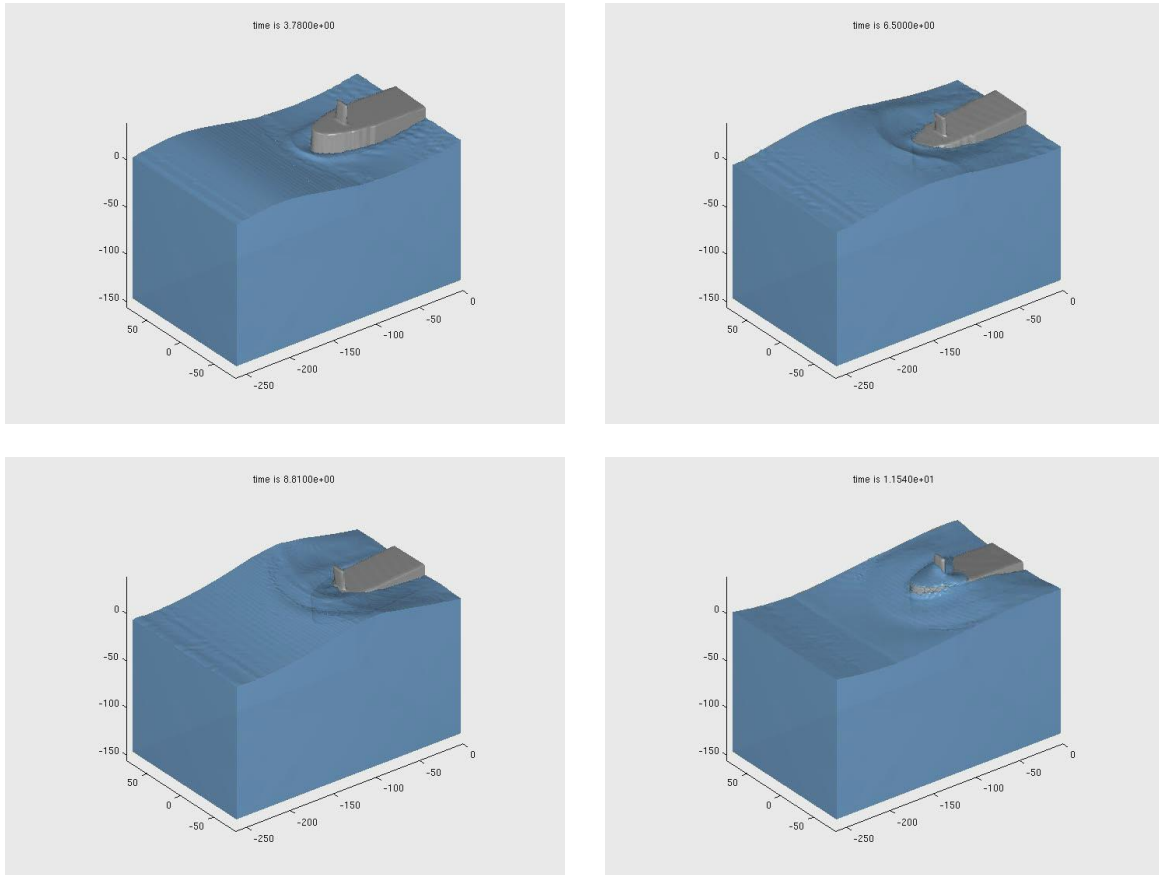
Figure 14: Snapshots of half of an FPSO shipping green water

has just flowed onto the deck (left figure), the agreement between the experiment and the simulation is reasonable. The moment in time the wave probe gets wet is almost the same. But in the first periods, the water height is somewhat higher in the simulation, whereas the total time the water hits the wave probe is shorter. Closer to the deck structure, in the right of Figure 16, the total amount of water passing the wave probe is much smaller in the simulation. This same behaviour can be seen from the pressure on the deck and the deck structure. Whereas the pressure at the deck, just behind the fore point of the FPSO agrees reasonably well, the pressure at the deck structure is much lower, indicating that in the simulation only a small amount of fluid reaches the deck structure. The velocity of the water on the deck is quite well predicted by the simulation. The moment in time the water reaches the deck structure is almost exactly the same in experiment and simulation.

There can be several reasons for the differences between simulation and experiment. Firstly, the grid may not be fine enough to simulate the flow on the deck correctly. The vertical size of a cell at the deck is about 0.5 m, implying that there are at most 10 cells in the water height. Further, there can still be a problem with the phase between the
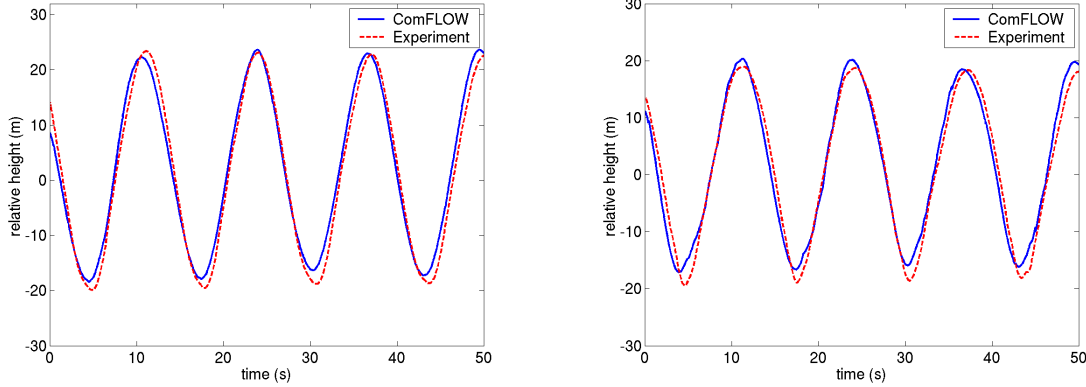
Figure 15: Relative wave height 30 meter (left) and 5 meter (right) in front of the FPSO
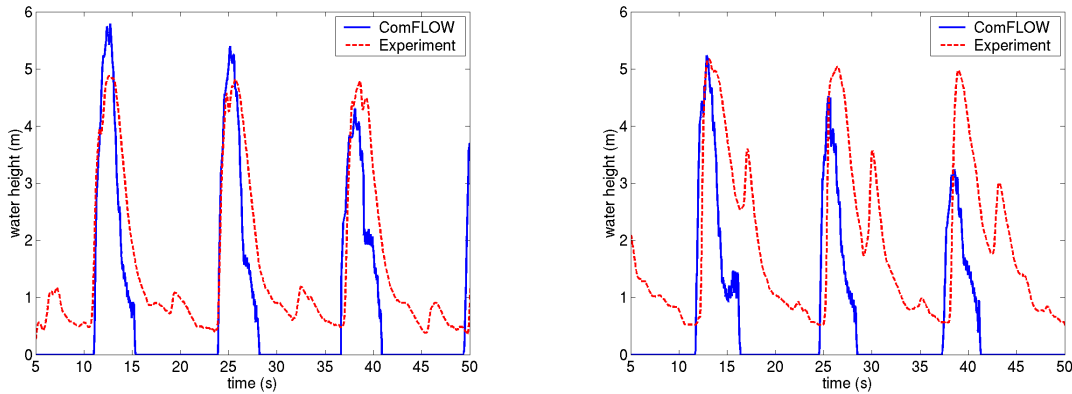

Figure 16: Water height on the deck of the FPSO: at the fore side of the bow (left) and near the deck structure (right)

wave and the motion of the vessel which are both prescribed, although this difference seems to be small when looking at the good agreement in Figure 15. To check that, a fully interactive simulation should be performed, where the motion of the vessel is not prescribed, but calculated during the simulation. At the moment, this is not feasible, but in the future this option will be available. One last reason could be the geometry of the ship, which is not exactly the same in the simulation as in the experiment.

7   CONCLUSIONS

In this paper, a numerical method is described for the prediction of local impact loads on floating structures. The method is based on a cut-cell approach on a fixed Cartesian grid, and is stable even when very small cells appear. For the displacement of the free surface, an improved VOF method is used, which results in full mass conservation.

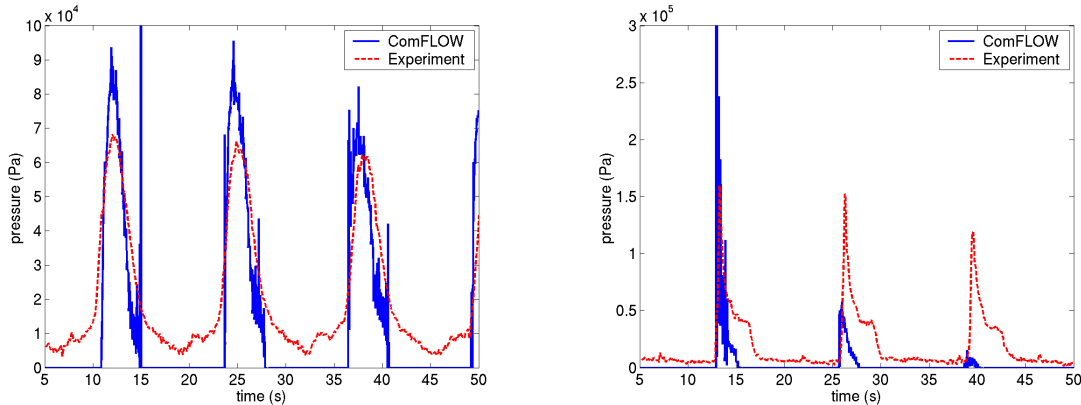Results have been shown of the wave elevation in a steep wave event which are com-

Figure 17: Left: pressure on the deck of the FPSO; right: pressure at the deck structure

pared with experimental measurements. The wave has been started using linear wave components, following from measurements at a wave probe. The development of the wave in the simulation is very well comparable with the experiment. The method is able to simulate a steep wave. Furthermore, a simulation of a breaking dam flow has been performed. The water height at several places in the domain and pressures at a box in the flow have been compared with measurements, showing a good agreement, especially in the first stage of the simulation. The global behaviour of the flow is the same in simulation and experiment. Finally, a very demanding simulation of high waves resulting in green water on the deck of a prescribed moving FPSO has been performed. The results show a reasonable agreement with measurements at the start of the simulation. But when the water is flowing onto the deck, the agreement becomes less. Improvement is needed using grid refinement, or a fully coupled simulation of ship motion and fluid flow.

In the further development of the method, already a start has been made with making it a two-phase model. A big advantage is that in two-phase models, no boundary conditions for the velocities are needed at the free surface, which are difficult to determine. In the coming years, the method will also be extended with a coupling to an outer domain where waves are generated using a much cheaper diffraction code. In this way, the ComFLOW domain can be limited to the near surroundings of the places of impact.

8 ACKNOWLEDGMENT

18

REFERENCES

[1] E.F.F. Botta, M.H.M. Ellenbroek. A Modified SOR Method for the Poisson Equation in Unsteady Free-Surface Flow Calculations. *J. Comp. Phys.*, **60**, 119–134, 1985.

[2] G. Fekken, B. Buchner, A.E.P. Veldman. Simulation of green-water loading using the Navier-Stokes equations. J. Piquet, editor. *Proc. 7th Int. Conf. on Numerical Ship Hydrodynamics*, 6.3-1-6.3-12, Nantes, 1999.

[3] G. Fekken. *Numerical Simulation of Free-Surface Flow with Moving Rigid Bodies*. PhD thesis, University of Groningen, 2004. URL: http://www.ub.rug.nl/eldoc/dis/science/g.fekken.

[4] J. Gerrits. *Dynamics of liquid-filled spacecraft*. PhD thesis, University of Groningen, The Netherlands, 2001, URL: http://www.ub.rug.nl/eldoc/dis/science/j.gerrits.

[5] J. Gerrits, A.E.P. Veldman. Dynamics of liquid-filled spacecraft. *J. Eng. Math.*, **45**, 21–38, 2003.

[6] F.H. Harlow, J.E. Welch. Numerical calculation of time-dependent viscous incompressible flow of fluid with free surface. *Phys. Fluids*, **8**, 2182–2189, 1965.

[7] C.R. Hirt, B.D. Nichols. Volume of fluid (VOF) method for the dynamics of free boundaries. *J. Comp. Phys.*, **39**, 201–225, 1981.

[8] G.E. Loots, B. Hillen, A.E.P. Veldman. The role of hemodynamics in the development of the outflow tract of the heart. *J. Eng. Math.*, **45**, 91–104, 2003.

[9] W.J. Rider, D.B. Kothe. Reconstructing volume tracking. *J. Comp. Phys.*, **141**, 112–152, 1998.

[10] R.W.C.P. Verstappen, A.E.P. Veldman. Symmetry-preserving discretization of turbulent flow. *J. Comp. Phys.*, **187**, 343–368, 2003.

[11] J. Westhuis. *The numerical simulation of nonlinear waves in a hydrodynamic model test basin*. PhD thesis, University of Twente, 2001.